FLORIDA STATE UNIVERSITY

COLLEGE OF ARTS AND SCIENCES

PREDICTABILITY OF THE PENINSULAR FLORIDA WET SEASON

By

CARLY D. NAROTSKY

A Thesis submitted to the
Department of Earth, Ocean, and Atmospheric Science
in partial fulfillment of the
requirements for the degree of
Master of Science

2021

Carly D. Narotsky defended this thesis on March 16, 2021.
The members of the supervisory committee were:

Vasubandhu Misra
Professor Directing Thesis

Alyssa Atwood
Committee Member

Mark Bourassa
Committee Member

Jeffrey Chagnon
Committee Member

The Graduate School has verified and approved the above-named committee members, and certifies that the thesis has been approved in accordance with university requirements.

TABLE OF CONTENTS

LIST OF FIGURES

ABSTRACT

Late spring or early summer brings an abrupt onset of a wet season to Peninsular Florida (PF). High daily rain rates are sustained throughout the summer until the demise of the wet season in autumn. Prediction of the Peninsular Florida Wet Season (PFWS) is important for Florida's agriculture industry, wildfire management, and water resource management. The onset and demise of the PFWS coincide with seasonal changes in the nearby ocean and atmospheric circulations, including the seasonal migration of the North Atlantic subtropical high (NASH). Yet, predictability of summer season precipitation in PF remains low compared to that of the winter season, which has a teleconnection with ENSO. This paper includes a skill assessment of the Community Climate System Model, version 4 (CCSM4) in predicting 1983–2015 summer season precipitation in PF, as well as the dates of onset and demise of the PFWS, using metrics of deterministic and probabilistic skill at hindcast lead times of 0–11 months. In the deterministic skill perspective, CCSM4 shows low skill in predicting the summer season precipitation and the dates of onset and demise of the PFWS, with high error values, low correlation, and high ensemble spread. CCSM4 has a late bias in predicting the onset and demise dates of the PFWS, and the late bias of the onset dates increases with hindcast lead time. For the probabilistic skill assessment, Relative Operating characteristic Curves (ROCs) are employed. The ROC scores indicate that CCSM4 may be skillful in predicting early onsets and late demises of the PFWS at some lead times but show no skill in predicting late onsets or early demises of the PFWS. Hindcasts of total seasonal rainfall amounts are generally unskillful, regardless of how the season is defined. Motivated by the role of the seasonal migration of the NASH in the timing of the onset of the PFWS and the finding of a late bias in the prediction of the onset of the PFWS, this paper also includes an analysis of CCSM4's ability to resolve the position and strength of the NASH at the time of the onset of the PFWS. CCSM4 strongly underestimates the observed interannual variability in the westward extent of the NASH at the time of the onset of the PFWS. This failure to resolve the position of the NASH at the time of the onset of the PFWS may be a contributing reason for the low predictability of the onset of the PFWS by CCSM4.

CHAPTER ONE

INTRODUCTION

1.1 What is the peninsular Florida wet season and why is it important?

Peninsular Florida (PF) experiences a distinct wet season during boreal summer. Each spring there is an abrupt onset of higher daily rain rates which are sustained through the summer and have an abrupt demise in autumn (Misra et al. 2018). These summer rains replenish the Floridan aquifer, a source of drinking water for the growing population of Florida and its neighboring states (Lindsey et al. 2009). The PF Wet Season (PFWS) also sustains the unique ecosystem of the Everglades and the storm protection, tourism, and fish that come with it (NWF 2019). Additionally, PFWS is vital for Florida's agriculture industry, which leads the nation in the production of seven crops, supports two million jobs, and contributes over $120 billion in economic impact to the state annually (Putnam 2016). Predicting the onset and the demise of the PFWS is of practical use to farmers choosing planting dates to optimize crop yields. Prediction of the onset of the PFWS is also valuable to land managers and policy makers who control wildfires, as the largest fires occur within a week of the onset of the PFWS (Slocum et al. 2007).

1.2 Seasonality of peninsular Florida, wet season variations and trends

Misra et al. (2018) analyzed the seasonal cycle of the upper ocean circulations and upper ocean heat content of PF's surrounding oceans using ocean heat transport, SST, and the depth of the 26°C isotherm. The researchers found that the onset of the PFWS accompanies the seasonal warming of the surrounding oceans and the strengthening of the Loop Current. Likewise, the demise of the PFWS occurs with a weakening of the Loop Current and a reduction in upper ocean heat content (Misra et al. 2018). An analysis of the wind field revealed a shift in wind patterns as well. At and prior to onset date, the 850 hPa level winds over PF are mostly northerlies and northwesterlies, but during the PFWS, the southerlies and southwesterlies that comprise the western edge of the North Atlantic subtropical high (NASH) prevail over PF (Misra et al. 2018). Low-level convergence resulting from the afternoon sea breezes on the east and west sides of PF accounts for much of the summer rainfall (Byers and Rodebush 1948; Bastola and Misra 2013). An analysis of the diurnal cycle of rainfall by Schwartz and Bosart (1979) revealed afternoon maxima across most of PF. The primary determinant for the magnitude of convergence is the differential heating between land and water over south Florida (Pielke

1974). Outflows from previous storms frequently trigger new growth (Cooper et al. 1982). Tropical cyclones also contribute to PFWS rainfall (Misra et al. 2018).

The climatological onset and demise dates of the PF wet season (PFWS) over 1948–2005 are May 21st and October 10th, respectively (Misra et al. 2018). These dates have large interannual variability; the standard deviation for the onset and demise dates are 15 and 16 days, respectively (Misra et al. 2018). As a result of this, there is considerable interannual variability in the length of the PFWS. Seasons with early onset dates, late demise dates, or that are longer than normal tend to correspond with positive seasonal rainfall anomalies (Misra et al. 2018). Therefore, predicting the onset and demise dates of the PFWS is useful for anticipating seasonal rainfall anomalies.

Observations show a decreasing trend in Florida wet season precipitation over the period 1892–2008 (Irizarry-Ortiz et al. 2011). This decreasing trend may be a result of a delayed onset, which is supported by the observation that the month of May showed the most pronounced decrease (Irizarry-Ortiz et al. 2011). Martinez et al. (2012) found statistically significant negative trends in May precipitation over Florida from 1970–2009 and in October precipitation from 1895–2009. Because typical onset and demise dates fall in May and October, respectively, these precipitation trends might suggest a trend toward later PFWS onset dates and earlier demise dates. However, Misra et al. (2018) found statistically insignificant linear trends in the timeseries' of onset dates, demise dates, and the length of PFWS. A modeling study by Marshall et al. (2004) examined the impacts of land-use changes in PF during the 20th century, including urbanization and conversion to agricultural land, on Florida's July-August precipitation. Due to the land-use changes over the course of the 20th century, the surface sensible and latent heat fluxes changed considerably, altering surface-forced mesoscale circulations such as afternoon seas-breezes. As a result, the spatial distribution of convective rainfall over PF was altered and the total July-August precipitation area-averaged over PF decreased (Marshall et al. 2004).

1.3 Predictability

There is a lack of predictability of precipitation in the PFWS in comparison to the winter season, which has a robust teleconnection with ENSO (Stefanova et al. 2012). Prior to 1976, ENSO variability influenced the PFWS too. Warm ENSO events in boreal winter preceded long wet seasons with an early onset, whereas cold ENSO events preceded short wet seasons with a late onset. Post-1976, however, the influence of ENSO on the PFWS has diminished (Misra and

DiNapoli 2013). This may be explained by a decadal change in the dynamics of the development of El Niño events (Wang 1995; Wang and An 2002; Wang and Picaut 2004). The warm SST anomalies associated with El Niño events in the pre-1976 period first occurred in the eastern tropical Pacific during boreal spring of the El Niño year and then spread westward. Post-1976, however, El Niño events began with warm SST anomalies in the western and central Pacific and the warming in the eastern Pacific occurred in the boreal spring following the El Niño year. After 1976, interannual variations in the PFWS have been found to be driven by variability of the North Atlantic Subtropical High (NASH; Li et al. 2011) and the size of the Atlantic Warm Pool (Misra and DiNapoli 2013).

1.4 Outline

Presented here is an assessment of the ability of the Community Climate System Model, version 4 (CCSM4; Gent et al. 2011) to predict the annual cycle of rainfall in PF, and, more specifically, the onset and demise of the PFWS. Also included is an analysis identifying a possible explanation of the model skill results by investigating CCSM4's depiction of the NASH at the time of the onset of the PFWS. All model analyses are performed at lead times of 0–11 months. Metrics of deterministic skill are used, including root mean square error, anomaly correlation, and signal-to-noise ratio. Additionally, probabilistic skill is assessed. Chapter 2 describes the data sources and methods used in this study, including the diagnosis of the dates of onset and demise of the PFWS. Chapters 3 and 4 detail the deterministic skill results and probabilistic skill results, respectively. Chapter 5 motivates and describes an analysis of CCSM4's depiction of the NASH during the PFWS. Chapter 6 offers conclusions.

CHAPTER TWO

DATA & METHODOLOGY

2.1 Diagnosing the onset and demise of the peninsular Florida wet season

The onset and demise dates are diagnosed using cumulative rainfall anomaly plots, a technique that was developed by Camberlin and Diop (2003) for defining the wet season in Senegal and has since been used in studies of wet seasons around the world (Slocum et al. 2010; Noska and Misra 2016; Misra et al. 2018). Examples of such plots are provided in Fig. 2.1. Daily rainfall is area-averaged over PF and the climatological annual mean rainfall is calculated. Daily rainfall anomalies are obtained by subtracting the climatological annual mean from the daily rainfall. The daily anomalies are cumulatively summed over the course of one calendar year. The onset date of the PFWS is the date on which the minimum of the cumulative sum occurs. The demise date of the PFWS is the date on which the maximum of the cumulative sum occurs, with the condition that the demise date must occur after the onset date.

Observed onset and demise dates of the PFWS 1983–2015 are calculated using daily precipitation data obtained from the CPC Global Unified Gauge-Based Analysis of Daily Precipitation (CPC Daily Precipitation; Higgins et al. 2000). Model-based onset and demise dates of the PFWS 1983–2015 are calculated also, using model CCSM4 hindcasted daily precipitation data at lead times of 0–11 months.

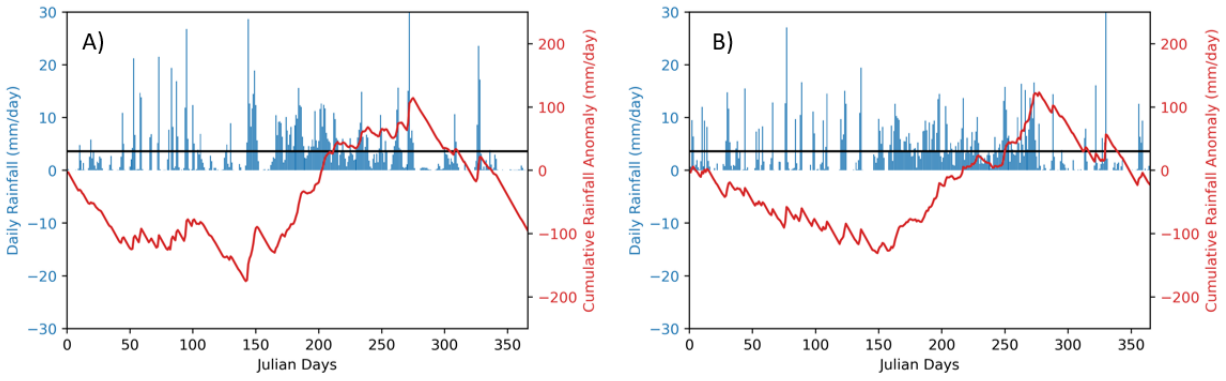

Figure 2.1. A) The illustration of the diagnosis of the onset and demise dates of the peninsular Florida wet season from observations for 1984, showing the daily area-averaged rainfall over peninsular Florida (blue bars), the annual mean climatology (black line), and the corresponding cumulative rainfall anomalies (red line). B) As in (A), but for 2014.

2.2 Data

CPC Daily Precipitation is a gauge-based precipitation dataset based on quality-controlled daily station reports, optimally interpolated with orographic consideration (Chen et al. 2008). The dataset is available with a spatial resolution of 0.5° latitude × 0.5° longitude over global land and with daily fields from 1979 to present.

The model assessed in this study is CCSM4; its precipitation hindcasts are compared to the observed CPC Daily Precipitation dataset. CCSM4 is a member of the North American Multimodel Ensemble (Kirtman et al. 2014). Ensembles of 10 year-long hindcasts are initialized on the first day of each month using the operational Climate Forecast System Reanalysis ocean, land, and atmospheric states (Kirtman et al. 2014). The daily precipitation data are available with a spatial resolution of 1.0° latitude × 1.0° longitude from 1982–2015.

2.3 Metrics of skill

The CCSM4 hindcast onset and demise dates are computed in each of the 10 ensemble members at lead times of 0–11 months. At each lead time, the ensemble mean onset dates and demise dates are computed for each year, and from those, the climatological onset dates and demise dates are computed. The climatological onset and demise dates from the CCSM4 hindcasts are compared to the observed climatological onset and demise dates of the PFWS (Fig. 3.1). The model hindcast onset and demise dates are compared to the observed onset and the demise dates by also employing the root mean square error (RMSE; Equation 1; Fig. 3.2) and the anomaly correlation, defined simply as the Pearson product-moment correlation between the observed and model hindcast onset dates or demise dates 1983–2015 (Fig. 3.3). The RMSE is also used to compare the CCSM4 hindcast monthly precipitation to the observed monthly precipitation (Fig. 3.5).

$$RMSE = \sqrt{\frac{\sum_{i=1}^{n}(\hat{y}_i - y_i)^2}{n}} \quad (1)$$

To assess the spread of the ensemble members, the signal-to-noise ratio is employed. The signal-to-noise ratio procedure is from Shukla et al. (2000). It is calculated as the variance of the signal (Equation 5) divided by the variance of the noise (Equation 3), using Equations (2)–(5) and a seasonal climate variable x_{ij} for N years (i=1, 2, 3 ,…, N) and n ensemble members (j=1, 2, 3,…, n). For this study, N=33 (for years 1983–2015) and n=10. The signal-to-noise ratio is

calculated for the model hindcasted onset dates and demise dates at lead times of 0–11 months (Fig. 3.4), and monthly mean rainfall at lead times of 0–11 months. (Fig. 3.6).

$$\bar{x}_i = \frac{1}{n}\sum_{j=1}^{n} x_{ij}\,; \quad \bar{\bar{x}} = \frac{1}{nN}\sum_{i=1}^{N}\sum_{j=1}^{n} x_{ij} \tag{2}$$

$$\sigma^2_{\text{noise}} = \frac{1}{N(n-1)}\sum_{i=1}^{N}\sum_{j=1}^{n}(x_{ij} - \bar{x}_i)^2 \tag{3}$$

$$\sigma^2_{\text{EM}} = \frac{1}{N-1}\sum_{i=1}^{N}(\bar{x}_i - \bar{\bar{x}})^2 \tag{4}$$

$$\sigma^2_{\text{signal}} = \sigma^2_{\text{EM}} - \frac{1}{n}\sigma^2_{\text{noise}} \tag{5}$$

Probabilistic skill is examined with relative operating characteristics, a useful technique for quantification of uncertainty in a hindcast or forecast. Kirtman (2003) advocates for the use of probabilistic verification as a complement to deterministic verification for its ability to quantify uncertainty. Here, it is employed in a manner following Graham et al. (2000) and Misra (2004). It is used to quantify CCSM4's skill in predicting early onset events, late onset events, early demise events, late demise events, high seasonal rainfall events, and low seasonal rainfall events. For the seasonal rainfall events, the seasonal rainfall is defined in three ways: June-July-August (JJA) rainfall, May-June-July-August-September (MJJAS) rainfall, and from the onset date to the demise date of the PFWS in each year. Thresholds for early and late onset and early and late demise dates are identified by ranking and separating the observed and hindcast onset and demise dates into terciles. For each year, the ensemble members are sorted into the contingency table (Table 1). For each ensemble member, values of H, M, FA, and CR are summed over all years, and the Hit Rate (HR; Equation 6) and False Alarm Rate (FAR; Equation 7) are computed. The HR and FAR are plotted against one another, creating Relative Operating Characteristic Curves (ROCs). The area under the ROC is a measure of probabilistic skill and is called the ROC score; ROC scores above 0.5 indicate a skillful hindcast.

This procedure is used for early and late onset and demise events at hindcast lead times of 0–11 months and for high and low seasonal rainfall events at hindcast lead times of 0–11 months.

$$HR = \frac{H}{H+M} \tag{6}$$

$$FAR = \frac{FA}{FA+CR} \tag{7}$$

Table 1. Contingency table used for creating relative operating characteristic curves to quantify hindcast uncertainty.

	Ensemble probability for event exceeds threshold.	Ensemble probability for event does not exceed threshold.
Event is observed. "Yes"	Hit (H)	Miss (M)
Event is not observed. "No"	False Alarm (FA)	Correct Rejection (CR)

CHAPTER THREE

RESULTS: CCSM4 DETERMINISTIC SKILL

3.1 Comparing CCSM4 hindcasts to observations

The observed climatological onset date of the PFWS during the study period 1983–2015 is June 1st, and its climatological demise date during the same period is October 6th (Fig 3.1). The 1983–2015 climatological onset dates hindcasted by CCSM4 have a late bias (Fig 3.1). As the hindcast lead time increases, the late bias of the onset dates increases. At a lead time of 0 months, the climatological onset date from the CCSM4 hindcast is June 4th, just 3 days later than the observed climatological onset date for the same time period. At a lead time of 1 month, the hindcasted climatological onset date jumps by 2 weeks to June 18th. At lead times of 2–5 months, the hindcasted climatological onset date hovers in the week of July 1st–5th, an error of approximately 1 month. The error increases again for lead times of 6–10 months, with hindcasted climatological onset dates of July 11th–14th. Finally, at a lead time of 11 months, the hindcasted climatological onset date of the PFWS is July 20th, an error of 49 days (Fig 3.1).

Like the onset dates, the 1983–2015 climatological demise dates hindcasted by CCSM4 also have a late bias (Fig 3.1). At a lead time of 0 months, the climatological demise date hindcast by CCSM4 is October 23rd, more than 2 weeks later than the observed climatological demise date, October 6th. The late bias increases with increasing lead time, with a late bias of 24 days at a lead time of 1 month, and a late bias of 28 days at a lead time of 2 months. At lead times of 3 months or more, the hindcasted demise dates remain consistently between November 4–8, an error of approximately 1 month (Fig. 3.1).

Unlike weather events, the onset and the demise dates of the PFWS is part of the seasonal cycle. As indicated in Misra et al. (2018) the onset and the demise of the PFWS coincides with corresponding seasonal changes in the upper ocean of the Gulf of Mexico and in the large-scale upper air circulations. Therefore, the forecast of these dates at seasonal time scale is plausible given its close ties to the seasonal cycle. This is partially demonstrated by the CCSM4 hindcasts showing relatively smaller errors in the forecast of climatological onset date and demise dates at short lead times. The fact that the errors of the CCSM4 hindcasts in forecasting the climatological onset and demise dates grow with lead time, suggests that the model drift is significant.

The anomaly correlation is used as one of the metrics of assessing the fidelity of CCSM4 hindcasts in forecasting the onset and the demise dates of the PFWS (Fig. 3.2). In a sobering display, CCSM4 hindcasts show that the anomaly correlations are very low at all lead times for both the onset dates and the demise dates, and there is no relationship to the hindcast lead time.

Another metric to measure the performance of the CCSM4 hindcast in forecasting the onset and demise dates of the PFWS is the RMSE (Fig. 3.3). The RMSE increases with increasing hindcast lead time for both the onset and the demise dates of the PFWS. It may be noted that the RMSE of the onset dates is generally higher than that of the demise dates.

The RMSE of the monthly mean precipitation area-averaged over PF is also computed at hindcast lead times of 0–11 months (Fig. 3.4). The highest RMSEs are in months during the wet season, particularly in June, July, August. In those months, the RMSE increases with increasing lead time. In most other months, there is no relationship between hindcast lead time and the RMSE of monthly mean precipitation.

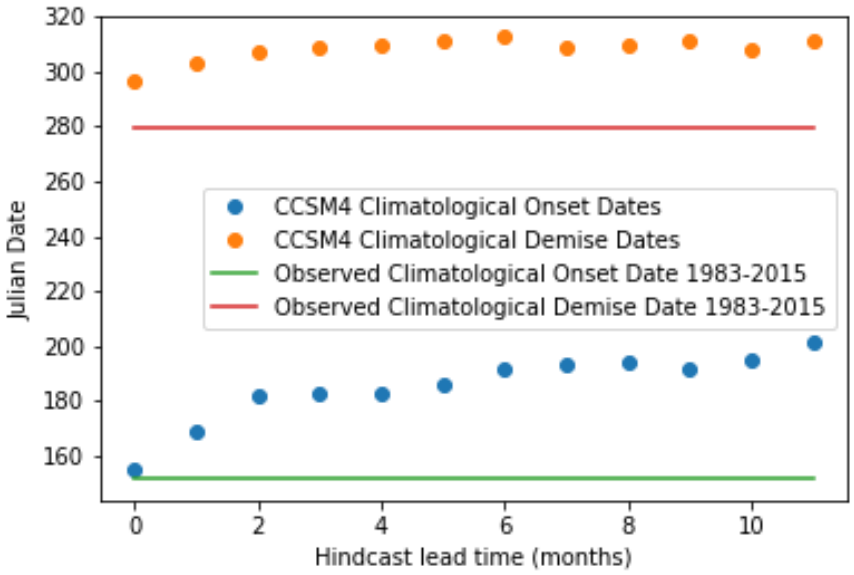

Figure 3.1. The observed 1983–2015 climatological onset date (green line) and demise date (red line) of the peninsular Florida wet season. The CCSM4 hindcast 1983–2015 climatological onset (blue dots) and demise (orange dots) dates of the peninsular Florida wet season at hindcast lead times of 0–11 months.

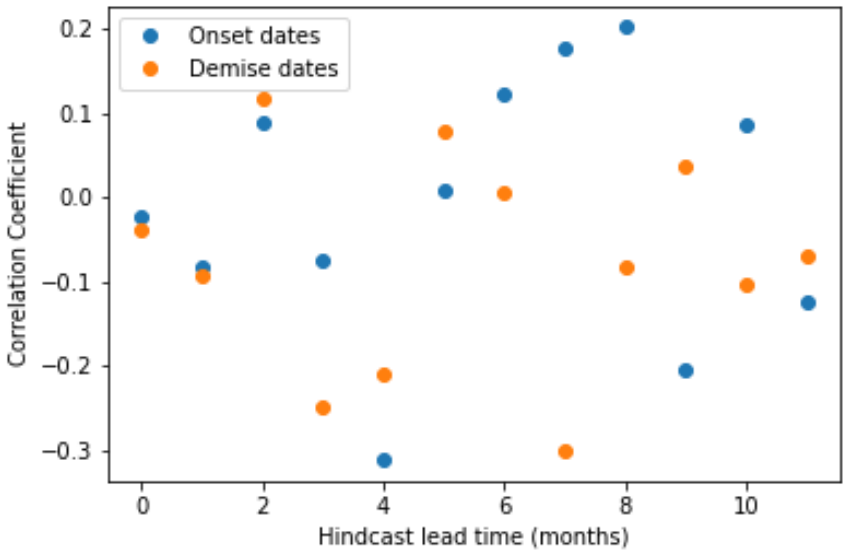

Figure 3.2. The anomaly correlation between the 1983–2015 observed and CCSM4 hindcast onset dates (blue dots) and the anomaly correlation between the 1983–2015 observed and CCSM4 hindcast demise dates (orange dots) of the peninsular Florida wet season.

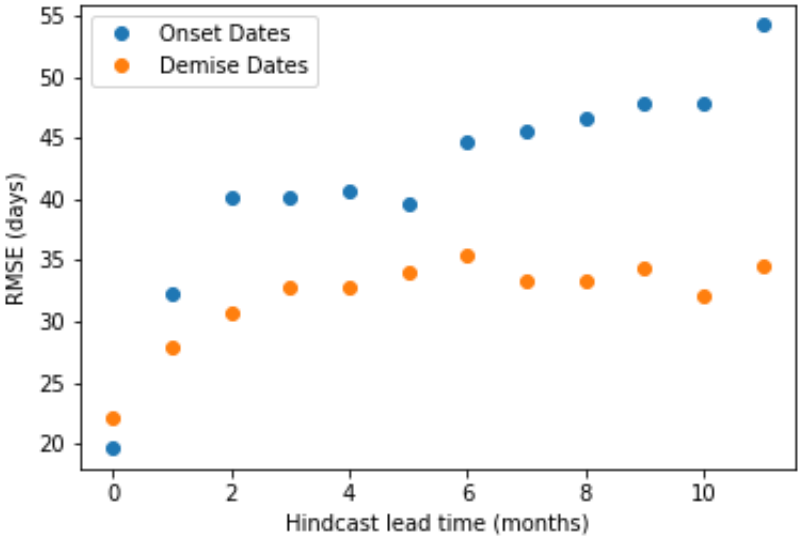

Figure 3.3. The root mean square error (RMSE) of the 1983–2015 onset dates (blue dots) and demise dates (orange dots) of the peninsular Florida wet season hindcast by CCSM4 at hindcast lead times of 0–11 months.

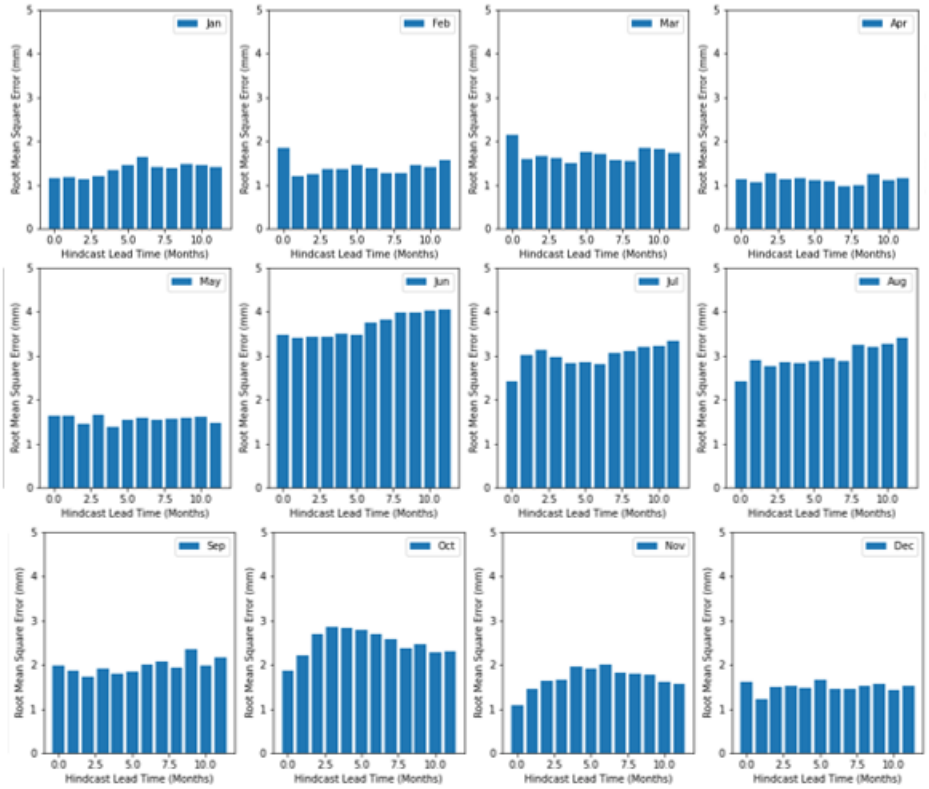

Figure 3.4. Root mean square error (RMSE) of monthly mean precipitation hindcast by CCSM4 at lead times of 0–11 months.

3.2 Ensemble spread

Precipitation data is stored for ten ensemble members per season in the CCSM4 hindcasts. These ensemble members are generated by perturbing the initial conditions (Kirtman et al. 2014). The signal-to-noise ratio is employed as a metric of the agreement of the ensemble. The higher the signal-to-noise ratio, the more the model runs agree with one another, and lower is the "ensemble spread". The signal-to-noise ratio is computed for the onset and the demise dates of the PFWS at hindcast lead times of 0–11 months (Fig. 3.6) and for the monthly mean precipitation at hindcast lead times of 0–11 months (Fig. 3.5). The signal-to-noise ratios for the onset and the demise dates of the PFWS are very low at all hindcast lead times (Fig. 3.6), indicating high ensemble spread in predicting the onset and the demise dates of the PFWS. The signal-to-noise ratios of the monthly mean precipitation are lowest during the months comprising the PFWS in most years, June–October (Fig. 3.5). Monthly mean precipitation in May and November, the months adjacent to the PFWS, have low signal-to-noise ratios, too. This indicates that ensemble spread for hindcasts of monthly mean precipitation is highest in the summer

months and lowest in the winter months. For all months, the signal-to-noise ratios for monthly mean precipitation generally decrease with hindcast lead time, indicating an increase in ensemble spread with hindcast lead time.

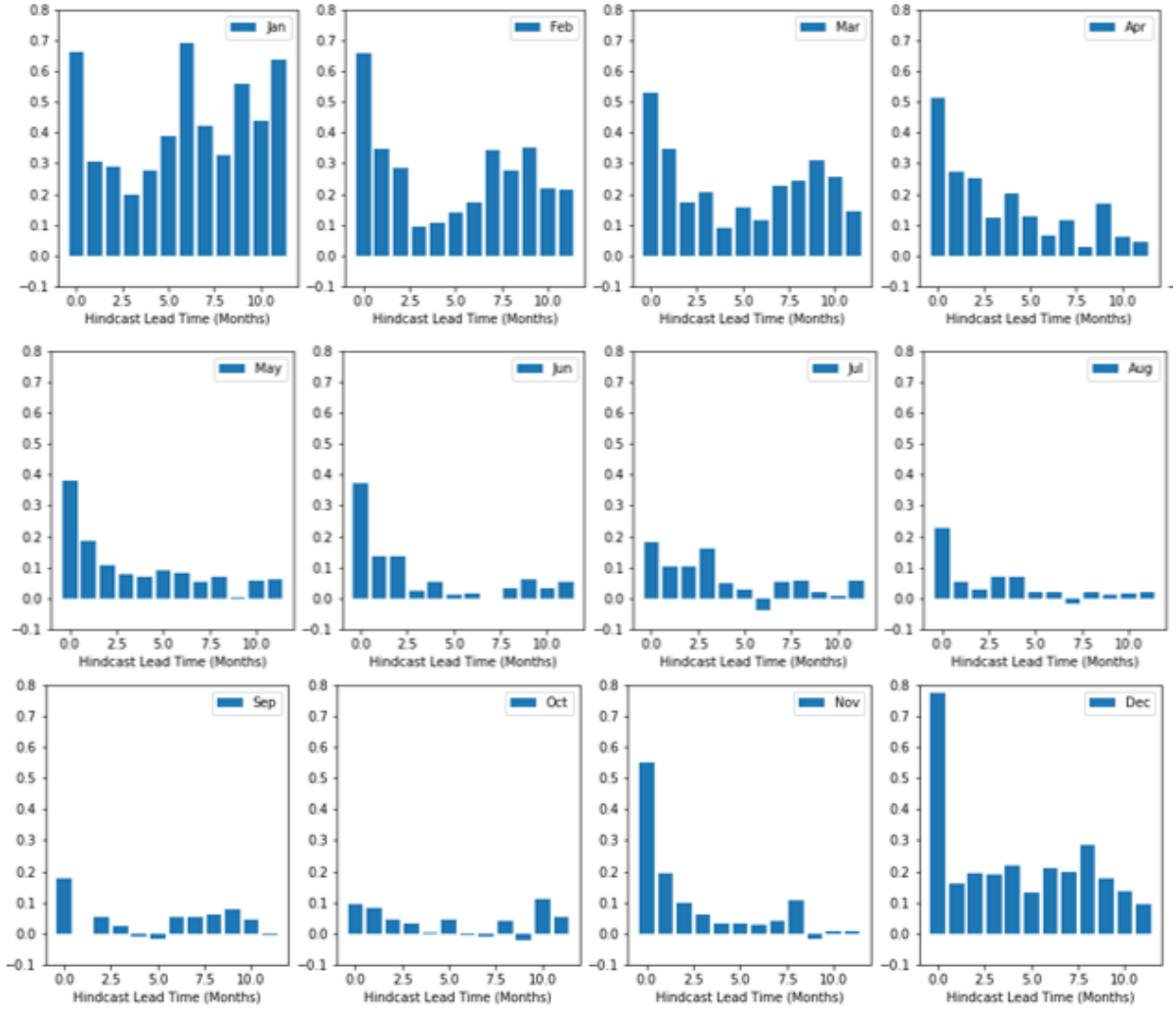

Figure 3.5. Signal-to-noise ratio of monthly mean precipitation hindcast by CCSM4 at lead times of 0–11 months.

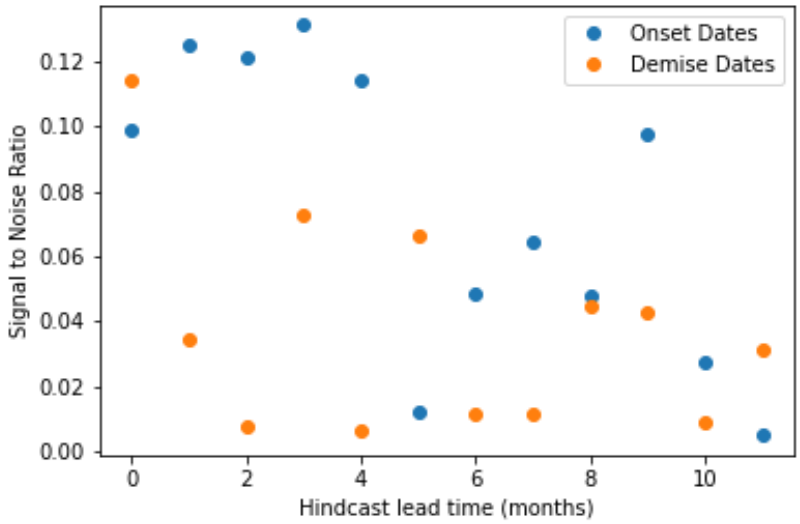

Figure 3.6. The signal-to-noise ratio of the CCSM4 hindcast onset dates (blue dots) and demise dates (orange dots) of the peninsular Florida wet season by lead time.

CHAPTER FOUR

RESULTS: CCSM4 PROBABILISTIC SKILL

4.1 Onset and demise dates of the peninsular Florida wet season

To assess the probabilistic skill of CCSM4 hindcasts in predicting the onset and the demise dates of the PFWS, ROC curves are created for hindcast lead times of 0–11 months for early onset events, late onset events, early demise events, and late demise events (Fig. 4.1). ROC curves that bow to the upper left of the plot represent a skillful hindcast. In other words, the hindcast is skillful if the area below the ROC is greater than 0.5. A hindcast is considered to have no skill or is no better than climatology or random forecast if the area under the ROC is below 0.5 (Graham et al. 2000). As such, the area under the ROC is a measure of the probabilistic skill of the CCSM4 hindcasts. These ROC skill scores reveal that CCSM4's predictions of early onset and late demise of the PFWS may be skillful at some lead times. However, CCSM4 is not skillful at predicting a late onset or an early demise of the PFWS (Fig. 4.2).

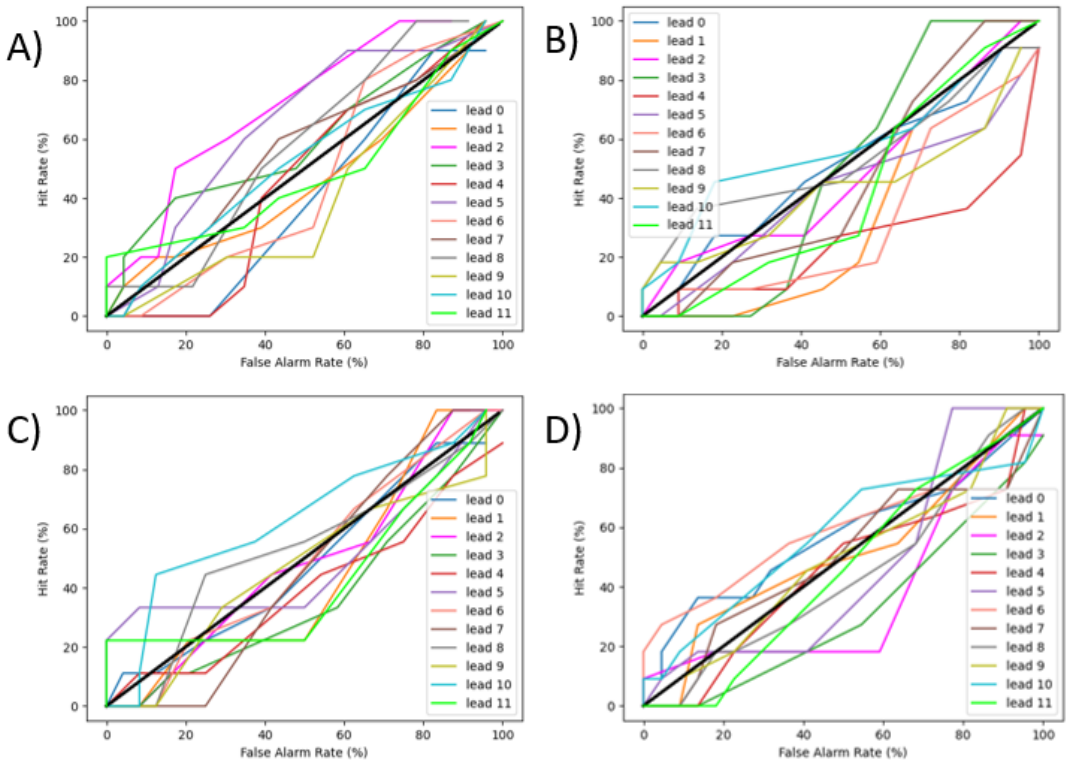

Figure 4.1. Relative operating characteristic curves for A) early onset events, B) late onset events, C) early demise events, and D) late demise events hindcast by CCSM4 at lead times of 0–11 months.

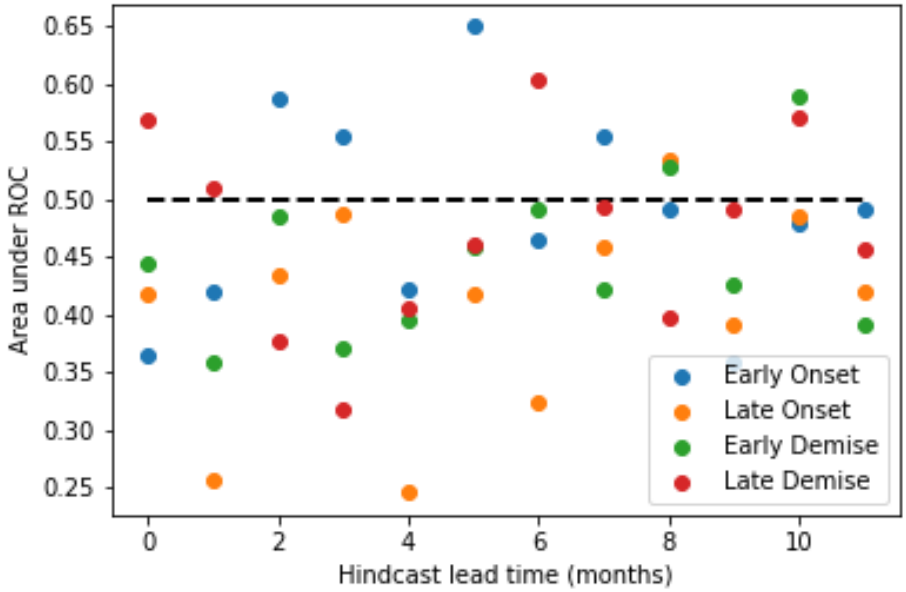

Figure 4.2. The area under the Relative Operating Characteristic Curve (ROC) for early onset events (blue dots), late onset events (orange dots), early demise events (green dots), and late demise events (red dots) from CCSM4 hindcasts at lead times of 0–11 months.

4.2 Seasonal rainfall

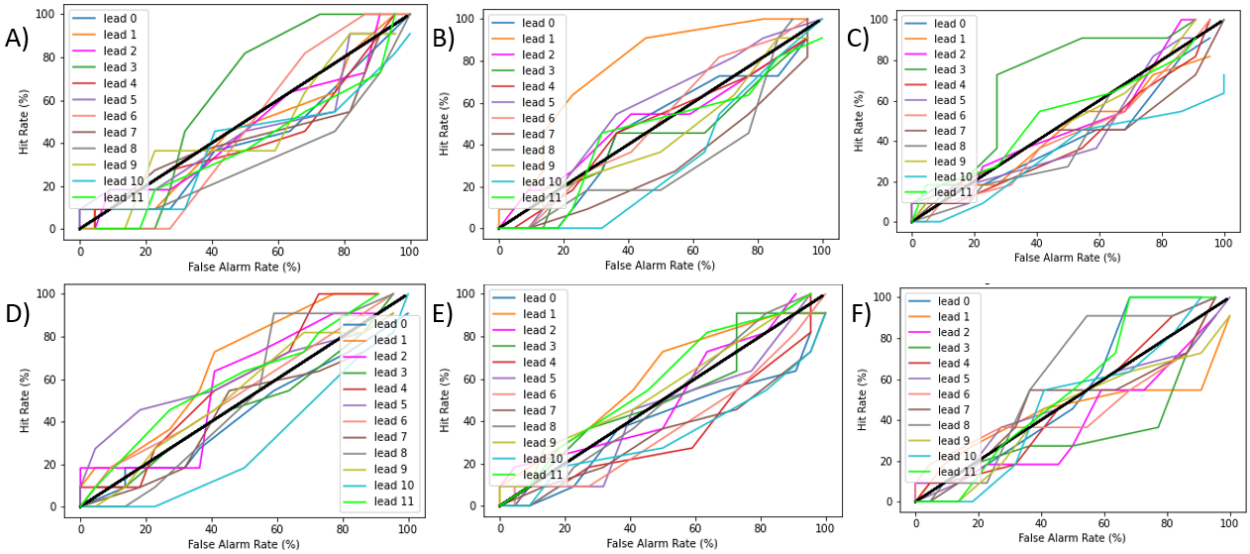

Figure 4.3. Relative operating characteristic curves for A) low June-July-August (JJA) rainfall events, B) low May-June-July-August-September (MJJAS) rainfall events, C) low PFWS (onset date to demise date) rainfall events, D) high JJA rainfall events, E) high MJJAS rainfall events, and F) high PFWS rainfall events hindcast by CCSM4 at lead times of 0–11 months.

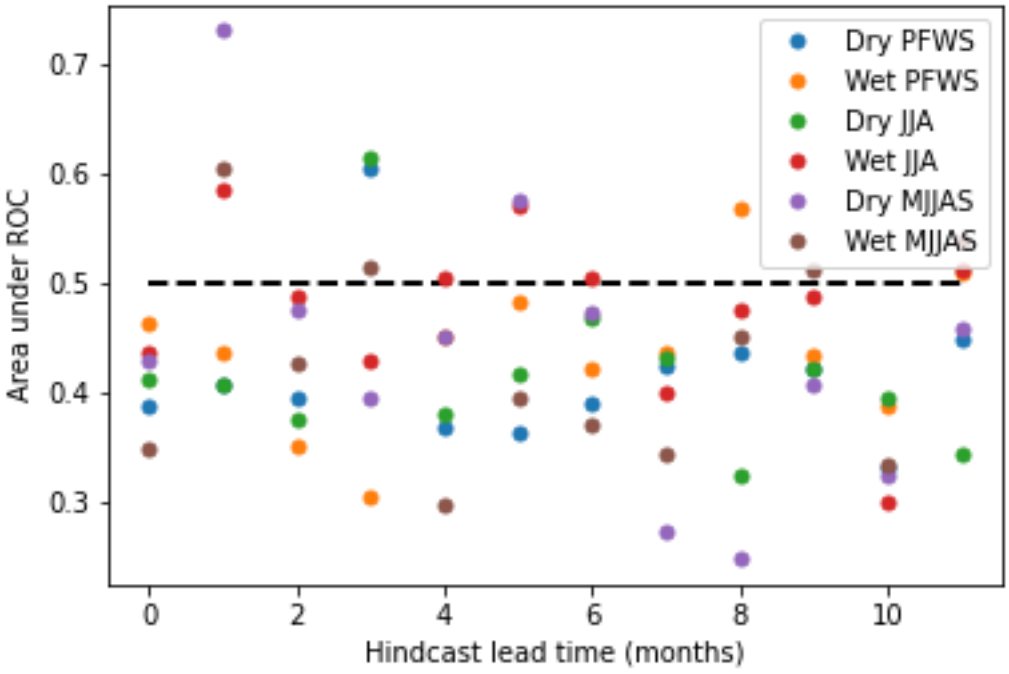

Figure 4.4. The area under the Relative Operating Characteristic Curve (ROC) for dry PFWS rainfall anomalies (with variable seasonal length; blue dots), wet PFWS rainfall anomalies (with variable seasonal length; orange dots), dry June-July-August (JJA) seasonal rainfall anomalies (with fixed season length; green dots), wet JJA rainfall anomalies (with fixed season length; red dots), dry May-June-July-August-September (MJJAS) seasonal rainfall anomalies (with fixed season length; purple dots), and wet MJJAS seasonal rainfall anomalies (with fixed season length; brown dots) for CCSM4 hindcasts at lead times of 0–11 months.

To assess the probabilistic skill of CCSM4 in predicting the seasonal rainfall of the PFWS, ROCs are created for hindcast lead times of 0–11 months for dry and wet seasonal rainfall anomalies (Fig. 4.3). The season is defined three ways: JJA, MJJAS, and the PFWS, which has a varying seasonal length as it starts on the onset date and ends on the demise date. The area under the ROC, i.e., the probabilistic skill scores, are calculated (Fig. 4.4). The area under the ROC skill scores show that CCSM4's predictions of summer seasonal rainfall anomalies, broadly construed, are generally unskillful, regardless of hindcast lead time.

CHAPTER FIVE

THE ROLE OF THE NORTH ATLANTIC SUBTROPICAL HIGH

5.1 Background and motivation

CCSM4 exhibits a late bias in predicting both the onset date and demise date of the PFWS. For the onset dates, the late bias increases with hindcast lead time (Fig. 3.1). The aim of the analysis within this chapter is to understand why this late bias exists.

The onset date and the demise date of the PFWS each coincide with changes in the prevailing 850 hPa wind direction over PF, associated with the seasonal migration of the NASH, as shown in Fig. 5.1 (Misra et al. 2018). Thirty days prior to the onset of PFWS, the mid-latitude westerlies are still present over PF. On the date of onset of the PFWS, a low-level trough is present over the western Atlantic Ocean, with northerly and northwesterly flow present in PF. The low-level trough may be accompanied by a trailing cold front, suggesting that the lifting mechanism provided by the synoptic frontal system triggers the onset of the PFWS. In the month following the onset date of the PFWS, the 850 hPa wind field in PF is dominated by the southerlies that comprise the western edge of the NASH. By autumn, the NASH retreats eastward. As the demise date of the PFWS approaches, the 850 hPa wind field in PF is no longer dominated by the NASH; instead, it is dominated by cyclonic flow, sometimes coincident with tropical cyclones (Fig. 5.2; Misra et al. 2018).

The goal of this analysis is to better understand the depiction of the NASH by CCSM4. Because the timing of the onset of the PFWS is tied to the seasonal migration of the NASH, the focus of the analysis presented here is the position of the NASH at the time of the onset of the PFWS.

5.2 Methodology

The analysis of the position of the NASH is performed using sea-level pressure data from the NCEP-DOE Reanalysis 2 (Kanamitsu et al. 2002) and CCSM4 model output at hindcast lead times of 0–11 months. The model data used is the ensemble mean, i.e., the mean over all ten runs. First, the strength of the NASH valid at the observed and model-hindcasted onset and demise dates of the 1983–2014 PFWSs is determined by finding the highest surface pressure value in the domain of the North Atlantic (280°–350° E and 15°–45° N). Secondly, of interest is the westward extent of the NASH at the time of the onset of the PFWS. This is analyzed by noting the location of the westernmost point of the 1020.0 hPa isobar within the North Atlantic

domain (280°–350° E and 15°–45° N). This analysis is performed using observed (NCEP-DOE Reanalysis 2) sea-level pressure valid on the observed onset dates, as well as using CCSM4 hindcasts of sea-level pressure at lead times of 0–11 months valid on the CCSM4 hindcasted onset dates at lead times of 0–11 months.

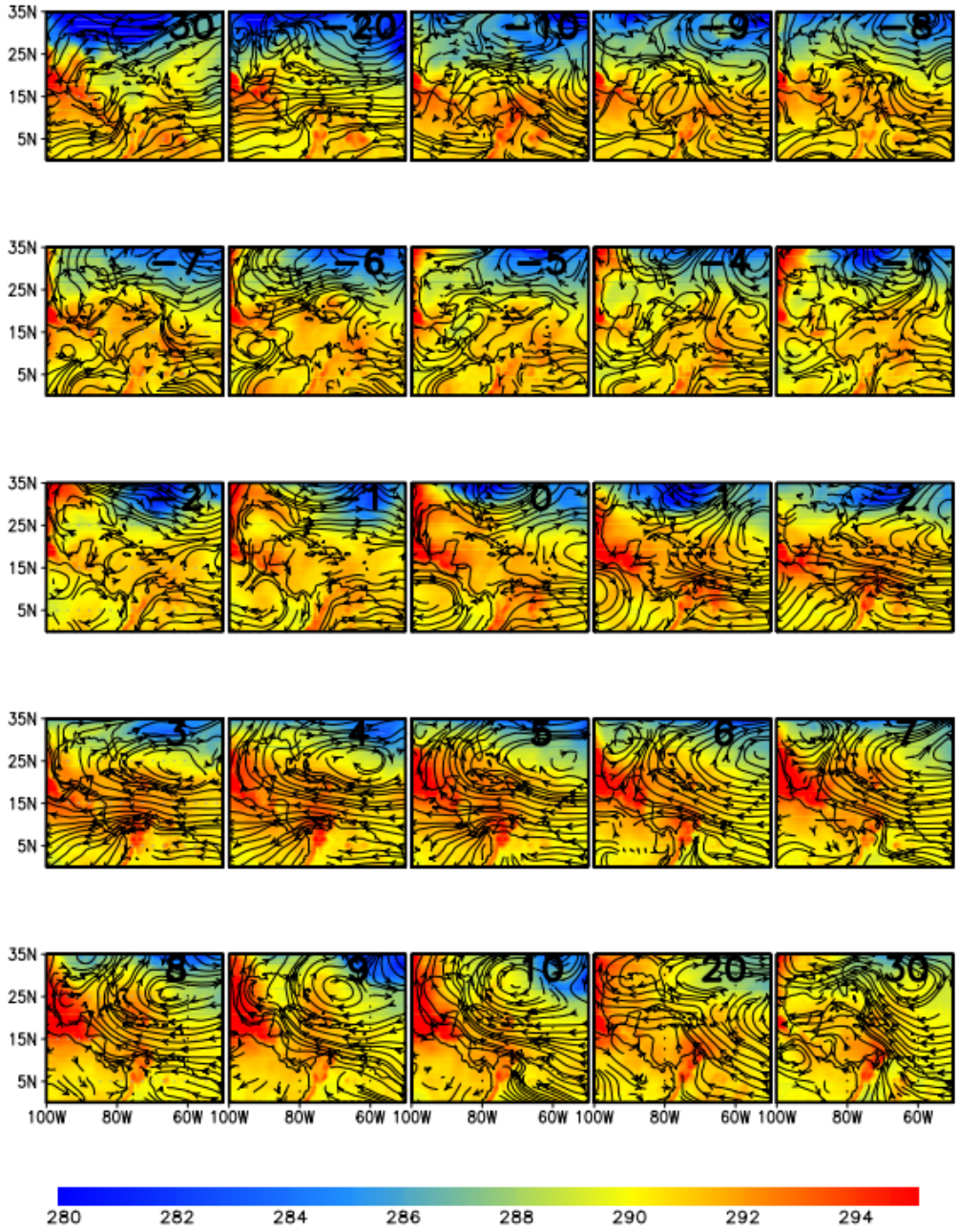

Figure 5.1. The composite evolution of the winds (m/s; streamlines) and the temperature (K; shaded) at 850 hPa 30 days prior and 30 days after onset of the PFWS. Reproduced from Misra et al. (2018).

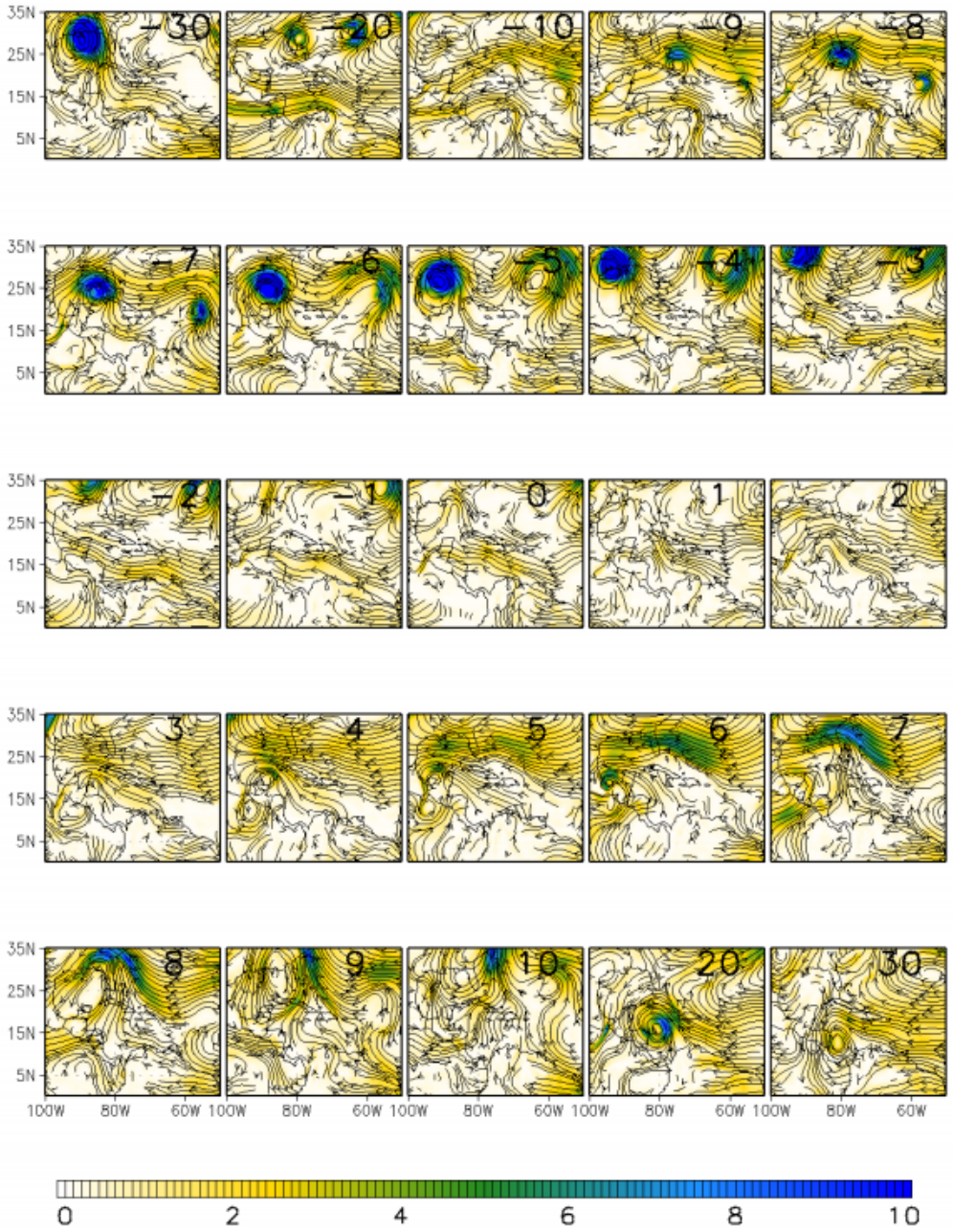

Figure 5.2. The composite evolution of the 850 hPa winds and the corresponding kinetic energy (shaded; m^2s^{-2}) 30 days prior and 30 days after demise of the PFWS. Reproduced from Misra et al. (2018).

5.3 Results

Fig. 5.3A shows that the maximum central pressure of the NASH on the observed onset dates falls between 1020 and 1035 hPa with large interannual variability. The observed central surface pressures valid on the onset dates hindcasted by the model at lead times of 0, 1, and 2 months also generally fall within the range of 1020–1035 hPa. Within the same year, there is

little coherence among the central pressure values on the various onset dates. This may be attributed to the fact that the observed and model hindcasted onset dates are each quite different from one another. The same is true for the demise dates (Fig. 5.3 B). There is little coherence between the central pressure values on the various demise dates of the same year. The range of maximum sea-level pressure values on the demise dates is approximately 1020–1035 hPa with large interannual variability, also.

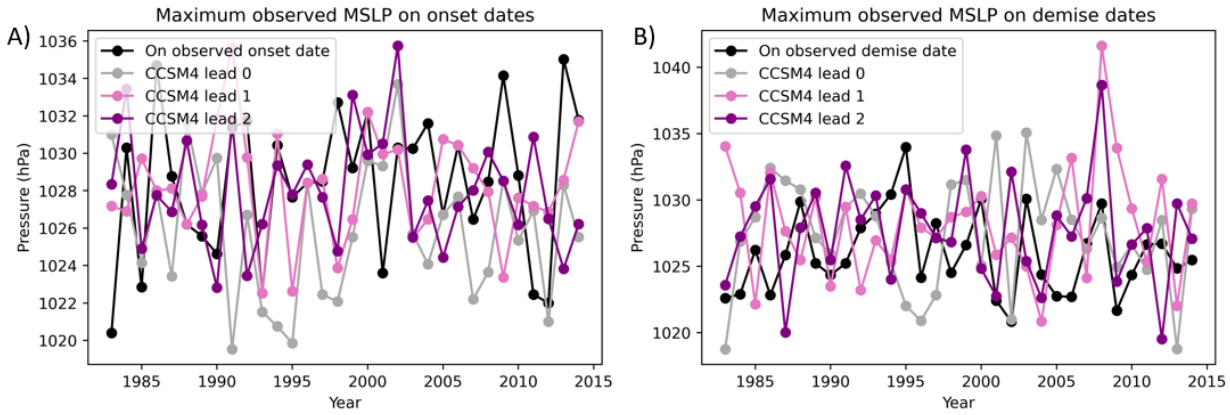

Figure 5.3. A) The observed maximum sea-level pressure in the domain 280°–350° E and 15°–45°, valid on the observed onset date (black line), and model CCSM4 onset date hindcasted at lead times of 0, 1, and 2 months (gray, pink, and purple lines, respectively). B) As in A), but valid on the demise dates.

The observed westernmost points of the 1020.0 hPa isobar on the observed onset dates of the 1983–2014 PFWSs are scattered in the southern and the western regions of the North Atlantic, indicating that the westward extent or migration of the NASH is highly variable interannually on the onset date of the PFWS (Fig. 5.4). At a hindcast lead time of 0 months, model CCSM4 shows that the westernmost point of the 1020.0 isobar is in the southwest region of the North Atlantic on the model-hindcasted onset dates in most years from 1983–2014 (Fig. 5.5 A). At hindcast lead times of 1–11 months, the westernmost point of the 1020.0 hPa isobar is in the southwestern region of the North Atlantic on all model-hindcasted onset dates from 1983–2014 (Fig. 5.5 B–L). CCSM4 erroneously predicts a lower interannual variability in westward extent of the NASH, an error that increases with increasing lead time.

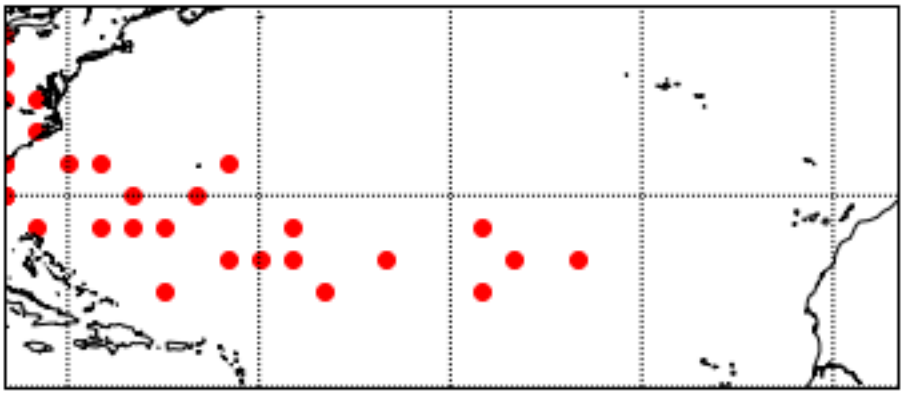

Figure 5.4. The observed westernmost points on the 1020.0 hPa isobar in the North Atlantic domain on the observed onset dates of the peninsular Florida wet season in 1983–2014.

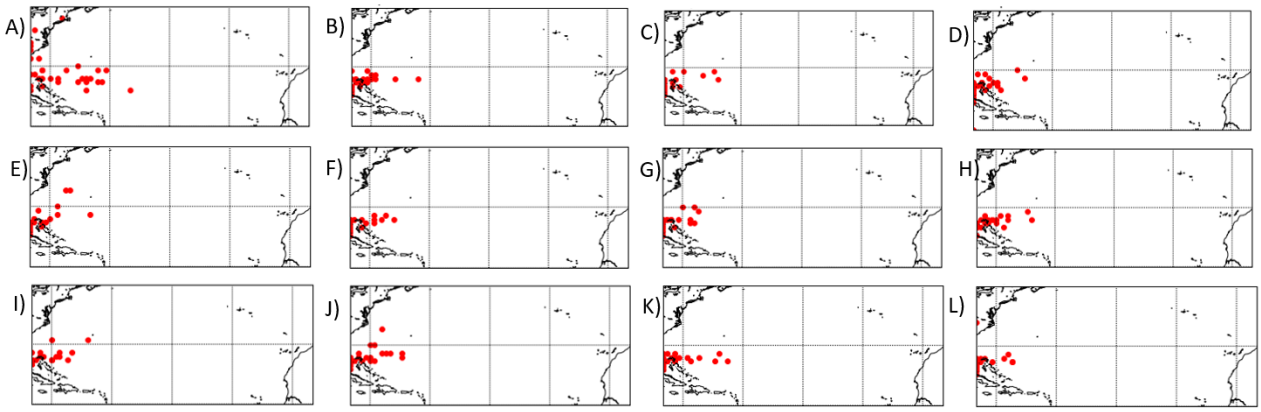

Figure 5.5. A) The westernmost point of the 1020.0 hPa isobar in the North Atlantic domain, hindcast by model CCSM4 at a lead of 0 months and valid on the 1983–2014 onset dates hindcasted by model CCSM4 at a lead time of 0 months. B–L) As in A), but at hindcast lead times of 1–11 months, respectively.

5.4 Discussion

The results of this project indicate that there is high interannual variability in the intensity of the NASH and in its westward extent on the date of the onset of the PFWS in the NCEP-DOE reanalysis. CCSM4 strongly underestimates the interannual variability of the westward extent on the date of the onset of the PFWS (Figs. 5.4 and 5.5). Li et al. (2011) suggest that the interannual variability in the meridional position of the NASH's western ridge is indicative of the interannual variability in summer precipitation in the southeast US. Li et al. (2011) analyzed the changes in the NASH from 1948–2007 using reanalyses and model simulations, and the results show that the interannual variability of the meridional position of the western ridge has increased in the last

30 years of the study period compared to the first 30 years, which has coincided with an increase in the interannual variability of precipitation in the southeast US over the last several decades. Li et al. (2011) further suggest that this increase in interannual variability—in both the position of the western edge of the NASH and the summer precipitation in the southeast US—may be expected to progress in the 21st century due to increasing atmospheric carbon dioxide concentrations. The researchers performed attribution analysis on the changes to the NASH that occurred over the 1948–2007 period, and the results suggest that the changes could likely be due to anthropogenic warming.

Future work is necessary to determine whether CCSM4 exhibits a systematic late bias in the timing of the seasonal evolution of the NASH. If this is found to be the case, one possible contributing reason for CCSM4's late bias in predicting the PFWS is that it also systematically produces a delay in the seasonal evolution of the NASH. To adequately assess CCSM4's depiction of the seasonal evolution of the NASH, further work must be performed that analyzes the NASH from boreal spring through autumn, not only on the date of the onset of the PFWS.

CHAPTER SIX

CONCLUSIONS

6.1 Conclusions regarding the skill of model CCSM4

The results of this study indicate that model CCSM4 has generally low predictive skill regarding the PFWS and summer precipitation in PF. CCSM4 has a late bias in predicting the onset and the demise dates of the PFWS (Fig. 3.1). For the onset dates only, the bias increases with hindcast lead time. The RMSE is high for the demise dates of the PFWS and even higher for the onset dates of the PFWS (Fig. 3.3). For the onset dates only, the RMSE increases with hindcast lead time. The late bias and RMSE of the demise dates of the PFWS remain constant at hindcast lead times greater than 1 month. Perhaps the most concerning finding is the extremely low anomaly correlations between the observed and CCSM4 hindcasted onset and demise dates of the PFWS (Fig. 3.2). However, in light of that, slightly comforting are the low signal-to-noise ratios of the hindcasts of the onset and demise dates of the PFWS (Fig. 3.5). Given the poor anomaly correlations and RMSE values, signal-to-noise ratios that indicate agreement among the ensemble members would be concerning.

The analyses of the RMSE and signal-to-noise ratio of the monthly mean precipitation in PF highlight the low predictability of summer precipitation in PF compared to the relatively high predictability of winter precipitation in PF (Figs. 3.4 and 3.6). This finding is consistent with previous studies which have noted the higher predictability of the winter season precipitation due to its teleconnection with ENSO (Stefanova et al. 2012). However, these analyses of the monthly mean precipitation in PF illuminate a potential concern regarding the predictions of February and March precipitation. For February and March monthly mean precipitation, the RMSE is highest at a hindcast lead time of 0 months, a surprising find, considering that errors are generally expected to increase with hindcast lead time. Furthermore, the signal-to-noise ratio of the monthly mean precipitation for February and March is highest at a hindcast lead time of 0 months, suggesting low ensemble spread and therefore, high confidence in the hindcast at that lead time. It is concerning that there is high confidence in a hindcast which resulted in large error.

The assessment of probabilistic skill showed that CCSM4 may have some skill predicting early onsets and late demises of the PFWS, but not late onsets or early demises of the PFWS

(4.2). Additionally, CCSM4 may have some skill predicting the quantity of seasonal precipitation when the season is defined with a fixed length, i.e., JJA or MJJAS (Fig. 4.4). However, this skill only appears at hindcast lead times of at least 1 month. The lack of skill at a lead of 0 months may be because the model needs spin-up time for the ocean and atmosphere to become coupled.

6.2 Conclusions regarding the North Atlantic subtropical high

This project highlights the interannual variability in the position of the NASH on the date of the onset of the PFWS. The westward extent of the NASH on the date of the PFWS onset can vary widely across the North Atlantic. However, model CCSM4 does not capture this interannual variability in the westward extent of the NASH. CCSM4 is remarkably persistent in its depiction of the westward extent of the NASH, with the westernmost point of the 1020.0 hPa isobar located in the southwest region of the North Atlantic on nearly all its hindcasted onset dates from 1983–2014. Furthermore, CCSM4 increasingly underestimates the interannual variability in the westward extent of the NASH with increasing lead time. Interannual variability in the position of the western ridge of the NASH contributes to interannual variability in summer precipitation in the southeast US, potentially including the PFWS. This suggests that a model's depiction of the interannual variability in the westward extent of the NASH is important for seasonal prediction of the PFWS. Underestimation of the interannual variability of the position of the western ridge of the NASH is a problem that may amplify as the interannual variability may continue to grow due to anthropogenic warming.

REFERENCES

Bastola, S., and V. Misra, 2013: Sensitivity of hydrological simulations of southeastern United States watersheds to temporal aggregation of rainfalls. *J. Hydrometeor.*, **14**, 1334–1344.

Byers, H.R., and H.R. Rodebush, 1948: Causes of thunderstorms of the Florida peninsula. *J. Meteor.,* **5**, 275–280, https://doi.org/10.1175/1520-04691948)005<0275:COTOTF>2.0.CO;2.

Camberlin, P., and M. Diop, 2003: Application of daily rainfall principal component analysis to the assessment of the rainy season characteristics in Senegal. *Climate Res.* **23**, 159–169.

Chen, M., P. Xie, and Coauthors, 2008: CPC Unified Gauge-based Analysis of Global Daily Precipiation, *Western Pacific Geophysics Meeting*, Cairns, Australia, 29 July–1 August, 2008.

Cooper, H.J., M. Garstang, and J. Simpson, 1982: The Diurnal Interaction Between Convection and Peninsular-Scale Forcing Over South Florida. *Mon. Wea. Rev.,* **110**, 486–503, https://doi.org/10.1175/1520-0493(1982)110<0486:TDIBCA>2.0.CO;2.

Gent, P. R., and Coauthors, 2011: The Community Climate System Model version 4. *J. Climate*, **24**, 4973–4991, doi:https://doi.org/10.1175/2011JCLI4083.1.

Graham, R. J., A. D. L. Evans, K. R. Mylne, M. S. J. Harrison, and K. B. Robertson, 2000: An assessment of seasonal predictability using atmospheric general circulation models. *Quart. J. Roy. Meteor. Soc.*, **126**, 2211–2240.

Higgins, R. W., W. Shi, E. Yarosh, and R. Joyce, 2000: Improved U.S. precipitation quality control system and analysis. NCEP/Climate Prediction Center Atlas **7**, 40 pp.

Irizarry-Ortiz, M.M., Obeysekera, J., Park, J., Trimble, P., Barnes, J., Park-Said, W. and Gadzinski, E., 2011: Historical trends in Florida temperature and precipitation. *Hydrol. Process.*, **27**, 2225–2246.

Kanamitsu, M., W. Ebisuzaki, J. Woollen, S.-K. Yang, J. J. Hnilo, M. Fiorino, and G. L. Potter, 2002: NCEP–DOE AMIP-II Reanalysis (R-2). *Bull. Amer. Meteor. Soc.*, **83**, 1631–1643, https://doi.org/10.1175/BAMS-83-11-1631.

Kirtman, B. P., 2003: The COLA Anomaly Coupled Model: Ensemble ENSO Prediction, *Mon. Wea. Rev*, **131**, 2324–2341.

Kirtman, B. P., and Coauthors, 2014: The North American Multimodel Ensemble: Phase-1 seasonal-to-interannual prediction; Phase-2 toward developing intraseasonal prediction. *Bull. Amer. Meteor. Soc*., **95**, 585–601.

Li, W., L. Li, R. Fu, Y. Deng, and H. Wang, 2011: Changes to the North Atlantic subtropical high and its role in the intensification of summer rainfall variability in the southeastern United States. *J. Climate*, **24**, 1499–1506. DOI: 10.1175/2010JCLI3829.1.

Lindsey, B.D., Berndt, M.P., Katz, B.G., Ardis, A.F., and Skach, K.A., 2009: Factors affecting water quality in selected carbonate aquifers in the United States, 1993–2005: U.S. Geological

Survey Scientific Investigations Report 20085240, 117 p.
https://pubs.er.usgs.gov/publication/sir20085240

Marshall, C.H., R.A. Pielke, L.T. Steyaert, and D.A. Willard, 2004: The Impact of Anthropogenic Land-Cover Change on the Florida Peninsula Sea Breezes and Warm Season Sensible Weather. *Mon. Wea. Rev.,* **132**, 28–52, https://doi.org/10.1175/1520-0493(2004)132<0028:TIOALC>2.0.CO;2

Martinez, C.J., Maleski, J.J., and M.F. Miller, 2012: Trends in precipitation and temperature in Florida, USA. *J. Hydrol.,* **452–453**: 259–281. doi:10.1016/j.jhydrol.2012.05.066

Misra, V., 2004: An Evaluation of the Predictability of Austral Summer Season Precipitation over South America, Journal of Climate, **17**, 1161–1175.

Misra, V., A. Bhardwaj, and A. Mishra, 2018: Characterizing the rainy season of Peninsular Florida. *Climate Dynamics*, **51**, 2157–2167, https://doi.org/10.1007/s00382-017-4005-2.

Misra, V., and S. M. DiNapoli, 2013: Understanding the wet season variations over Florida. *Climate Dynamics*, **40**, 1361–1372, https://doi.org/10.1007/s00382-012-1382-4.

National Wildlife Federation (NWF), 2019: The Everglades. Accessed 18 July 2019, https://www.nwf.org/Educational-Resources/Wildlife-Guide/Wild-Places/Everglades.

Noska, R., and Misra V., 2016: Characterizing the onset and demise of the Indian summer monsoon. *Geophys. Res. Lett.* **43**, 4547–4554.

Pielke, R.A., 1974: A Three-Dimensional Numerical Model of the Sea Breezes Over South Florida. *Mon. Wea. Rev.,* **102**, 115–139, https://doi.org/10.1175/1520-0493(1974)102<0115:ATDNMO>2.0.CO;2

Putnam, A. H., 2016: Florida Agriculture: By the Numbers., Florida Department of Agriculture and Consumer Services, Tallahassee, FL. https://www.nass.usda.gov/Statistics_by_State/Florida/Publications/Annual_Statistical_Bulletin/FL_Agriculture_Book/2016/Florida_Agriculture_by_the_Numbers_Brochure_2016.pdf

Schwartz, B.E. and L.F. Bosart, 1979: The Diurnal Variability of Florida Rainfall. *Mon. Wea. Rev.,* **107**, 1535–1545, https://doi.org/10.1175/1520-0493(1979)107<1535:TDVOFR>2.0.CO;2

Shukla, J., and Coauthors, 2000: Dynamical Seasonal Prediction. *Bull. Amer. Meteor. Soc*., **81**, 2593–2606.

Slocum, M. G., Platt, W. J., Beckage, B., Orzell, S. L., & Taylor, W., 2010: Accurate Quantification of Seasonal Rainfall and Associated Climate–Wildfire Relationships, *J. Appl. Meteor. and Clim.,* **49**, 2559–2573.

Slocum, M. G., W. J. Platt, B. Beckage, B. Panko, J. B. Lushine, 2007: Decoupling Natural and Anthropogenic Fire Regimes: A Case Study in Everglades National Park, Florida, *Natural Areas Journal*, **27**, 41–55.

Stefanova, L., V. Misra, J. J. O'Brien, E. P. Chassignet, and S. Hameed, 2012: Hindcast skill and predictability for precipitation and two-meter air temperature anomalies in global circulation models over the Southeast United States. *Climate Dynamics.*, **38**, 161–173. https://doi.org/10.1007/s00382-010-0988-7.

Wang, B., 1995: Interdecadal changes in El Niño onset in the last four decades, *J. Climate*, **8**, 267–285.

Wang, B., and S.-I. An, 2002: A mechanism for decadal changes of ENSO behavior: Roles of background wind changes, *Climate Dynamics*, **18**, 475–486.

Wang, C., and J. Picaut, 2004: Understanding ENSO physics—A review. *Geophys. Monogr.*, **147**, 21–48.

BIOGRAPHICAL SKETCH

Carly Narotsky was born in Durham, North Carolina in 1996 to her parents Kathy Kaufman and Mike Narotsky. As a teenager, she spent her summers working as a camp counselor at the Burgundy Center for Wildlife Studies in West Virginia, where she taught workshops on various nature topics; her favorite topics to teach were Weather and Butterflies. She got her start in meteorological research in the summer of 2017 at the National Weather Center Research Experience for Undergraduates (REU), working under Dr. Jason C. Furtado of the University of Oklahoma to study trends in the strength and position of the stratospheric polar vortex in the 20th and 21st centuries. Inspired by her REU experience and her younger brother's temporary move to Cañar, Ecuador, she designed and conducted a research project on the wet season of the Ecuadorian Andes with the guidance of Dr. Douglas K. Miller at the University of North Carolina at Asheville (UNCA). While a student at UNCA, she also worked as a private tutor in Atmospheric Sciences and as a field research assistant, helping to maintain a rain gauge network in Great Smoky Mountains National Park and launching rawinsonde weather balloons during wintry precipitation events in Asheville, NC. In 2018, she graduated Magna Cum Laude from UNCA with a B.S. in Atmospheric Sciences with a concentration in Climatology and a minor in Mathematics, receiving the Atmospheric Sciences Class of 2018 Academic Excellence Award and earning Distinctions in Atmospheric Sciences, as a University Scholar, and as a University Research Scholar. In 2019, she began her graduate studies at Florida State University, where she has been working under Dr. Vasubandhu Misra to study the wet season of peninsular Florida and working as a teaching assistant. Beyond her academic interests, she enjoys spending time with her pet tegu Titan, playing soccer, and being outdoors.